Interfacial quantum well states of Xe and Kr adsorbed on Ag(111)

J. D. McNeill, R. L. Lingle, Jr., R. E. Jordan, D. F. Padowitz,[a] and C. B. Harris[b]
Department of Chemistry, University of California, Berkeley, California 94720
and Chemical Sciences Division, Ernest Orlando Lawrence Berkeley National Laboratory, Berkeley, California 94720

(Received 22 January 1996; accepted 21 May 1996)

The energies and dispersions of the image states and quantum well electronic states in layers of Xe and Kr on a Ag(111) substrate were determined by angle-resolved two-photon photoemission (ARTPPE). For Xe, we measured binding energies of unoccupied electronic states for 1–9 layers and their parallel dispersion out to 4 layers. We measured the binding energies for a monolayer of Kr and dispersions for one and two layers. The $n=2$ and $n=3$ image states of the bare metal evolve into quantum well states of the layer (states of the Xe conduction band discretized by the boundary conditions of a 2-D slab) at higher Xe thicknesses, where the $n=2,3$ states exhibit both a perpendicular and parallel dispersion similar to that of the bulk Xe conduction band. The $n=1$ state appears to evolve with coverage as an image state screened by the Xe layer, with appreciable electron density in the vacuum. A continuum dielectric model (modified image state picture) reproduces the gross trends in the data, while an explicit quantum well analysis is used to extract the bulk Xe conduction band dispersion. A simple model which takes into account the band structures of the substrate and the overlayer, as well as the image potential, gives good agreement with the binding energy data. The combination of high energy and momentum resolution along both the surface parallel and surface normal yields very precise measurements of the bulk Xe conduction band as well as information about the behavior of conduction band electrons at interfaces. © *1996 American Institute of Physics.* [S0021-9606(96)00933-6]

I. INTRODUCTION

Solid Xe serves as a model system for understanding aspects of band structure and transport in both semiconductors[1] and insulators[2] due to its large band gap, high excess electron mobility, and the simple closed shell electronic structure of the Xe atom. Thus adlayers of noble gases on metals hold promise for understanding the electronic structure of ultrathin metal/semiconductor and metal/insulator interfaces. Also, the study of quantum well (QW) states associated with such layers should provide important information about the bulk band structure.[3] Recently, ultraviolet photoemission spectroscopy has been used to investigate the *occupied* quantum well electronic states in metal/metal,[4] metal/semiconductor,[5,6] and metal/insulator[7] systems. In this paper, we present angle-resolved two-photon photoemission (ARTPPE) spectra of the *unoccupied* quantum well and image states in the presence of insulating layers of Xe and Kr on Ag(111). Our ARTPPE spectrometer has a resolution of 7 meV and is well-suited to the study of surface and adsorbate states in the range of energies from slightly below the Fermi level up to the vacuum level. ARTPPE has been applied to a variety of metal and semiconductor surfaces yielding energies,[8–10] dispersions, and lifetimes[11–13] of excited states on the surface. The technique has also been used to study a monolayer of Xe where the changes in image state binding energy and dispersion were assigned to the work function shift due to adsorption and the polarization of the Xe layer.[14] ARTPPE investigations of layers of alkanes[15,16] revealed a sensitive dependence of the electronic structure on the layer thickness and the presence of localized electronic states. TPPE spectra of layers of metal on metal[17,18] have demonstrated the pinning of image states to the local work function, linewidth broadening due to lateral electron confinement on islands of adsorbate, and quantum well states.

The Xe/Ag(111) ARTPPE spectrum exhibits a complex dependence on coverage (Fig. 1) with several sharp spectral features, one of which becomes less bound at higher coverage while other features become more bound. The spectral feature which becomes less bound for thicker Xe layers is attributed to the $n=1$ image state of the layer, located primarily at the layer/vacuum interface. The $n=2,3$ image states become QW states of the layer at 7–9 layers of Xe and exhibit a mixed QW/image state behavior at intermediate coverage. In simplest terms, the attractive electron affinity of the Xe slab provides a shallow quantum well, bounded by the bulk band gap of the substrate on one side and the image potential on the other side. Since the spectra appear to display both image state and QW state characteristics over the range of experimental conditions, we offer interpretations of the data based these two viewpoints: a continuum dielectric (modified image potential) picture and an explicit quantum well model. Then we propose a simple model which attempts to account for the most important features identified in previous models: the band structure of the metal substrate, the band structure of the Xe overlayer, and the screened image potential of the adsorbate/metal system.

[a]Permanent address: Department of Chemistry, Amherst College, Amherst, MA 01002.
[b]Author to whom correspondence should be addressed.

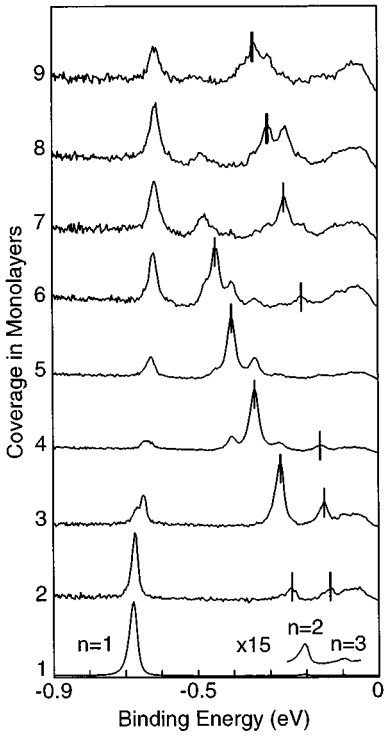

FIG. 1. Two-photon photoemission spectra of Xe/Ag(111) at a series of coverages (1–9 atomic layers, approximately). After two layers, the Xe coverage is non-uniform, and peaks corresponding to more than one coverage are visible in a given spectrum. The dark line through the peaks indicates which peak is assigned to the coverage (in monolayers) indicated at the left of the figure. A non-linear background was subtracted from the spectra in order to enhance the clarity of the features.

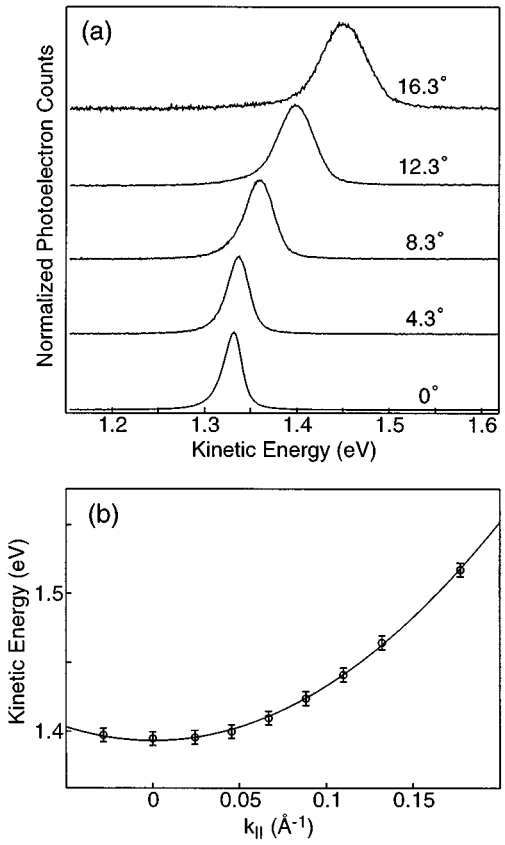

FIG. 2. In plot (a) spectra of the $n=1$ state of a monolayer of Xe on Ag(111) at a series of angles are displayed. The peak energy positions are used to determine the dispersion relation (see the text). In plot (b) reduced dispersion data for a monolayer of Xe on Ag(111) are shown along with a parabolic fit determining the experimental effective mass, yielding $m^*/m_e = 0.95 \pm 0.1$.

II. EXPERIMENTAL METHODS

Details of our experimental apparatus are published elsewhere[14] and are only briefly described here. A 2 MHz train of 6 ps pulses at wavelengths of 590–620 nm was generated by a synchronously-pumped, cavity-dumped dye laser. Second harmonic generation was achieved by means of a 2 mm BBO crystal. The laser was tuned so that the photon energy of the second harmonic was just below the work function in order to be able to investigate states near the vacuum level while keeping one-photon photoemission down to acceptable levels (below the point where space-charge broadening has a noticeable effect on the spectral features). The second harmonic and the residual fundamental beam were focused collinearly on the sample. The energies of emitted electrons were determined by a time-of-flight single-electron-counting spectrometer.

The parallel dispersion was measured by varying the angle of the sample with respect to the detector using a goniometer sector capable of angles between $-4°$ and $20°$. The angular acceptance of the detector was $\pm 1.6°$. Typical raw data is shown in Fig. 2 along with a typical dispersion relation. At a given angle θ the wave vector along the surface parallel $k_\parallel$ was determined from the sample angle and photoelectron kinetic energy E as follows:

$$k_\parallel = \sqrt{2m_e E/\hbar^2}\sin\theta. \tag{1}$$

A fit to the parabolic dispersion relation, $E = E_0 + \hbar^2 k_\parallel^2/2m^*$, where E_0 is the kinetic energy for emission normal to the surface, determined the effective mass m^*.

The sample was cooled as low as 45 K by means of a liquid helium cryostat. The UHV chamber background pressure was $\sim 1\times 10^{-10}$ Torr. Mono- and bilayer Kr and Xe were obtained by cooling the sample and backfilling the chamber with sample gas at pressures and sample temperatures specified by the phase diagrams of Kr and Xe on Ag(111).[19,20] At a Xe pressure of $\sim 2\times 10^{-6}$ Torr and at temperatures between 82–68 K a monolayer of Xe formed. At a Xe pressure of $\sim 2\times 10^{-6}$ Torr and a temperature of 67–66 K a bilayer formed. Experiments were performed quickly to minimize the effects of contaminants in the chamber or sample gas. Xenon multilayers were formed by carefully metered dosing of the cooled ($\sim$45 K) sample. The spectrum for a monolayer Xe grown by backfilling the chamber with Xe at temperatures and pressures specified by the 2-D phase diagram of Xe/Ag(111) was indistinguishable from the spectrum for a monolayer of Xe obtained by metered dosing at 45 K. This is consistent with Xe/Ag(111) x-ray structure results,[21] which show Xe to form an incommensurate hexagonal layer on the Ag(111) surface, whether

the layer is grown by metered dosing by time (nonequilibrium conditions) or by backfilling (equilibrium conditions).

The adsorption-induced work function shift changes the contact potential difference between the sample and detector which in turn changes the measured kinetic energy of the photoelectrons. In order to determine binding energies with respect to the vacuum, the work function change must be determined. The adsorbate-induced work function shift $\Delta\Phi$ was determined by TPPE and confirmed via threshold UPS. A fit of the UPS data to the Fowler form[22] determined the work function. The work function shift was determined from the TPPE spectrum by analyzing the convergence of the image series to the vacuum level using the quantum defect formula, $E=-0.85/(n+a)^2$, and simultaneously solving for the quantum defect a, the binding energy with respect to the vacuum E, and the position of the vacuum level (the energy to which the series converges), for both the clean and the adsorbate-covered surface. Then the energy difference between the vacuum level for the clean and adsorbate-covered surface yields the work function change due to the adsorbate. (The quantum defect formula can only be applied to the bare surface and the monolayer, where the states are still approximately hydrogenic. For bilayer, only UPS results were used.) The UPS and TPPE results for the work function change due to the monolayer agree to within 10 meV. Our results differed somewhat from other threshold photoemission work[23] in that we observed most of the work function difference occurring in the first layer ($\Delta\Phi=-0.500$ eV), with a small shift ($\Delta\Phi=-0.036$ eV) for the second layer, and no shift within experimental uncertainty for the third layer. We attribute this discrepancy to uncertainty in the determination of coverage in the previous work. The work function shift due to the presence of a monolayer of Kr was determined to be -0.30 eV.

III. COVERAGE DEPENDENCE OF THE SPECTRAL FEATURES

The TPPE spectra of Xe/Ag(111) at various thicknesses of Xe are presented in Fig. 1, and the binding energies of the $n=1,2,3$ states are plotted in Fig. 3 (the labels $n=1,2,3$ represent the image state levels to which the states correspond in the limit of zero coverage). The binding energies of the image states on a monolayer of Kr were determined to be -0.62 and -0.19 eV for $n=1$ and $n=2$, respectively.

For the first layer, the features are similar to the $n=1,2,3$ image states of clean Ag(111), as shown by Merry *et al.*[14] The $n=1$ feature on a monolayer of Xe is significantly narrower than that on the clean Ag(111) surface, suggesting a longer lifetime of the $n=1$ state in the presence of a layer of Xe. At the completion of a bilayer, the signal intensity of the $n=1$ peak is reduced relative to the $n=2,3$ features while the peak shifts to lower binding energy. The $n=2,3$ peaks, however, move to a slightly higher binding energy. Past the third layer, the binding energy of the $n=1$ peak changes very little with coverage, while the binding energy of the $n=2$ peak increases by 70 meV in going from three to four layers. The marked contrast between the coverage dependence of the $n=1$ peak and the $n=2,3$ peaks suggests that the states exist in different locations along the axis perpendicular to the surface. *The coverage dependence of the $n=1$ peak is characteristic of image states outside an insulating layer, whereas the coverage dependence of the $n=2,3$ states is characteristic of QW states of the Xe layer.*

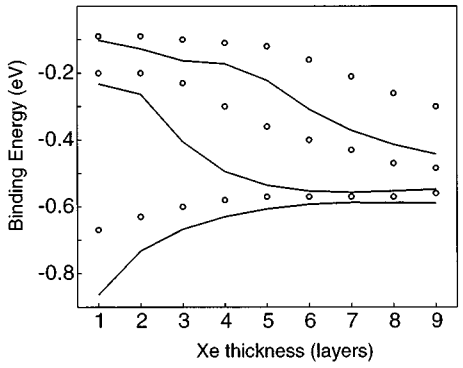

FIG. 3. Experimental binding energies (symbols) of the $n=1,2,3$ states as a function of Xe coverage, and a comparison to the results of a dielectric model (solid lines). Energies are with respect to the vacuum level. The dielectric model reproduces the trends in the data as a function of layer thickness but is quantitatively unsatisfactory.

The angular dependence of the TPPE features was determined for 1–4 layers of Xe and for one and two layers of Kr. The angle-resolved spectra of the $n=1$ state on a monolayer of Xe at a series of angles between 0° and 16° are shown in Fig. 2 along with the reduced parallel dispersion data with a parabolic fit. The coverage dependence of the effective mass of the $n=1,2$ states of Xe/Ag(111) is shown in Fig. 4. For both the $n=1$ and $n=2$ states, the effective mass goes from that of a free electron (0.95 ± 0.1 m_e for $n=1$) at monolayer coverage to significantly less than that of a free electron

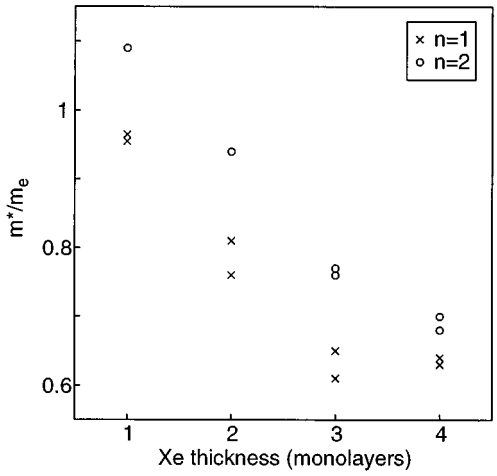

FIG. 4. Effective masses of $n=1$ and $n=2$ states as a function of Xe coverage. Data from two separate experiments are shown. See the text for uncertainty estimate.

(0.6 ± 0.2 m_e for $n=1$) at 4 layers of coverage. The $n=1$ effective masses for 1–2 layers of Kr follow the same trend as for Xe (0.9 ± 0.1 m_e for a monolayer, 0.8 ± 0.2 m_e for a bilayer).

IV. COMPARISON TO THEORY

The binding energy of the $n=1$ state decreases by 16% over the range of 1–9 layers. Most of this shift takes place over the first few layers. Such a decrease in binding energy with layer thickness has been observed for image states on n-alkanes,[15] which have a negative (repulsive) electron affinity[13] and where the electron density is located in the vacuum. Due to the similarity of the coverage dependence for $n=1$ on Xe/Ag(111) with the coverage dependence for $n=1$ observed on alkane layers, we assign the $n=1$ state to be an image state residing primarily at the Xe/vacuum interface. In contrast the binding energies of the $n=2,3$ states monotonically increase as the number of layers increases, in agreement with what is expected for QW states of the Xe conduction band. The energies of such QW states should approach the bulk Xe conduction band minimum for thicker layers. Thus we compare the data to the results of two types of models, each of which represents different assumptions as to the relative importance of the dielectric nature of the adsorbate and its band structure. The dielectric continuum model treats the adsorbate as a structureless dielectric. The QW models ignore dielectric effects within the layer and use bulk potentials in the layer.

A. Dielectric continuum model

To model image states perturbed by the presence of the dielectric layer, we have employed the well-established dielectric continuum model for image states outside an insulator layer on a perfect conductor, first presented along with numerical solutions by Cole.[24,25] An approximate analytic form for the wave function was developed by Trninić-Radja *et al.*[26] This model represents an attempt to account for the effect of the dielectric nature of the adsorbate (represented by a dielectric constant and an affinity level) on image state binding energies. Binding energies for image states on liquid He[27] and thin layers of alkanes on a metal[13] can be explained by this model. However, this model does not take into account the band structure of the layer, which should be important for states residing in the layer.

In the dielectric continuum model, the electrostatic potential on the inside of the dielectric slab as presented by Jackson[28] is given by

$$V_i(z)=-\frac{e^2}{4\epsilon z}+\frac{e^2(\epsilon-1)}{4\epsilon(\epsilon+1)(t-z)}-\frac{e^2(\epsilon-1)(t+2z)}{4\epsilon(\epsilon+1)t(t+z)}+\delta V_i(z)-\mathrm{EA}, \tag{2}$$

where z is the distance from the metal surface, t is the thickness of the layer, the electron affinity of the layer EA is treated as an additive constant and is set to the Xe conduction band value of 0.5 eV,[29] ϵ is the static dielectric constant of Xe, and the correction term is given by the infinite series

$$\delta V_i(z)=-\frac{e^2z^2}{2\epsilon t^3}\sum_{k=2}^{\infty}\frac{(-1)^k}{k(k^2-z^2/t^2)}\left(\frac{\epsilon-1}{\epsilon+1}\right)^k. \tag{3}$$

Numerical computation yields the following explicit approximation for $\delta V_i(z)$,

$$\delta V_i(z)\approx\delta V_i(t)\cdot\frac{z^2}{t^2}[1-0.55(1-z/t)+0.30(1-z/t)^2]. \tag{4}$$

The series for δV_i can be summed at $z=t$ to give,

$$\delta V_i(t)=\frac{e^2}{4\epsilon t}\left[\frac{(1+\beta)^2}{\beta}\ln(1+\beta)-\frac{3}{2}\beta-1\right]$$

$$\text{where } \beta=\frac{\epsilon-1}{\epsilon+1}. \tag{5}$$

The electrostatic potential in the vacuum, first presented by Cole,[25] can be written as,

$$V_o(z)=-\frac{e^2}{2(\epsilon+1)z}-\frac{e^2(\epsilon-1)}{4(\epsilon+1)(z-t)}+\delta V_o(z) \tag{6}$$

and the correction term is given by

$$\delta V_o(z)=-\frac{e^2\epsilon t}{(\epsilon+1)^2z}\sum_{k=1}^{\infty}\frac{(-1)^{k-1}k}{(kt+z)}\left(\frac{\epsilon-1}{\epsilon+1}\right)^k. \tag{7}$$

The correction term can adequately be approximated by

$$\delta V_o(z)\approx\frac{2t^2}{z(t+z)}\cdot\frac{\delta V_o(t)}{1+0.222\left(\frac{\epsilon-1}{\epsilon+1}\right)\cdot\ln(z/t)}, \tag{8}$$

where the value of δV_o at $z=t$ is given by

$$\delta V_o(t)=-\frac{e^2}{t}\left[\frac{\epsilon}{(\epsilon^2-1)}\cdot\ln\left(\frac{2\epsilon}{\epsilon+1}\right)-\frac{1}{2(\epsilon+1)}\right]. \tag{9}$$

Two steps were taken to avoid the singularities in the electrostatic solution at the interface. First, a cutoff was imposed at -4 eV near the metal, resulting in a bare metal binding energy of -0.75 eV which is close to the experimental value for clean Ag(111) of -0.77 eV. Second, the potential is linearly interpolated between $V(t-b/2)$ and $V(t+b/2)$ near the dielectric/vacuum interface. The Schrödinger equation incorporating this potential is solved by numerically integrating the wave function from the origin (where the wave function is set to zero, corresponding to a hard wall boundary at the metal) out to a large distance (130 Å) in the vacuum using a 4th and 5th order Runge–Kutta integrator with adaptive step sizes. The solutions are evaluated at large z over a range of energies to find solutions which vanish at large z and are eigenstates of the model potential.

The potential given by the dielectric model for $\epsilon=3.0$, EA$=0.5$ eV, and $b=3$ Å for various layer thicknesses is shown in Fig. 5. The resulting binding energies are shown in Fig. 3, plotted with the binding energies extracted from the

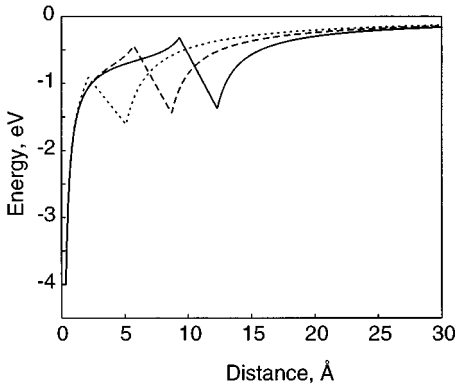

FIG. 5. The potential used in the dielectric model eigenenergy calculations. The potential is the solution to the electrostatic problem of an electron in or near a dielectric slab on a metal surface. The results for 1–3 layers of Xe (3.6 Å per layer, $\epsilon=3.0$) are shown. The image potential at the metal is cut off at -4 eV. The potential is linearly interpolated over a region of width $b=3$ Å at the Xe/vacuum interface.

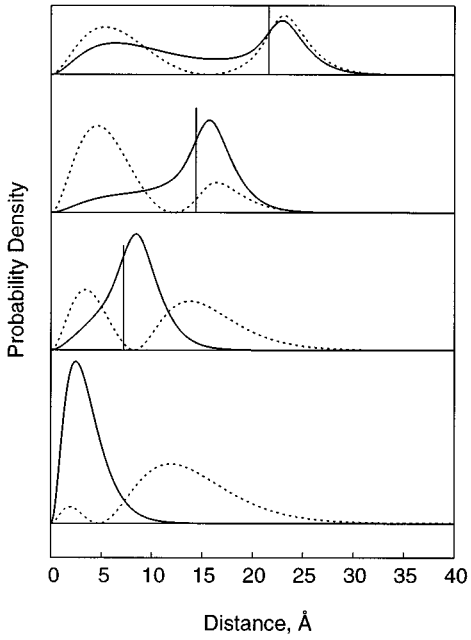

FIG. 6. The resulting probability densities for the dielectric continuum model for the $n=1$ (solid lines) and $n=2$ (dashed lines) states for 0,2,4, and 6 layers of a slab of dielectric constant $\epsilon=3.0$ and electron affinity EA$=0.5$ eV. This figure illustrates the tendency of the $n=1$ state to have significant electron density at the Xe/vacuum interface at these coverages while the $n=2$ state looks like a hydrogenic $n=2$ image state for a monolayer but tends to move inside the layer and have a node near the Xe/vacuum interface, which is indicative of a quantum well state, for thicker layers.

data of Fig. 1. Although the model overestimates the binding energies for all three states, it is significant that it does reproduce the major trends in the data: the $n=1$ image potential state energy becomes more positive while the higher quantum state energies become more negative as the adlayer thickness increases.

This has two implications. First, dielectric screening of the electron–metal interaction by the xenon slab is important for the $n=1$ electron. Second, the attractive potential represented by the EA term in Eq. (2) transforms the $n=2,3$ image states into quantum well states of the layer as thickness increases. This suggests that the $n=2,3$ energies should be analyzed by a model which takes explicit account of their quantum well character, as is done below. It is also interesting that the wave functions predicted by the continuum model show a tendency for the probability associated with the $n=1$ image potential electron to move out toward the adlayer/vacuum interface as shown in Fig. 6.

B. Discrete wave vector model for QW states

The energies of QW states can be analyzed to give information on the perpendicular dispersion of the bulk band from which they derive. According to the theory of Loly and Pendry,[3] QW wave functions possess a factor of $\sin k_z z$. For wave functions in a layer N atoms deep the wave function must vanish at $z=0$ and Nd, where d is the interplanar spacing, leading to the bound state condition $k_z=\pi j/Nd$, where j is the quantum number of the QW state. (Due to a different definition of the layer boundaries, Ref. 3 uses $N+1$ instead of N.) In the effective mass approximation the energy levels will follow the dispersion relation $E=\hbar^2 k_z^2/2m^*$. Thus the electronic energy levels of a quantum well can be thought of as a discretized band structure. If the energies of the states for a range of thickness are plotted against k_z, the perpendicular dispersion can be observed. The band structure information obtained by this analysis is complementary to band structure information obtained by angle resolved measurements of the parallel dispersion: By performing angle resolved measurements and coverage resolved measurements, a large area of the 3-D surface corresponding to the conduction band ($E(k_\parallel,k_z)$) can be determined. In Fig. 7 the bind-

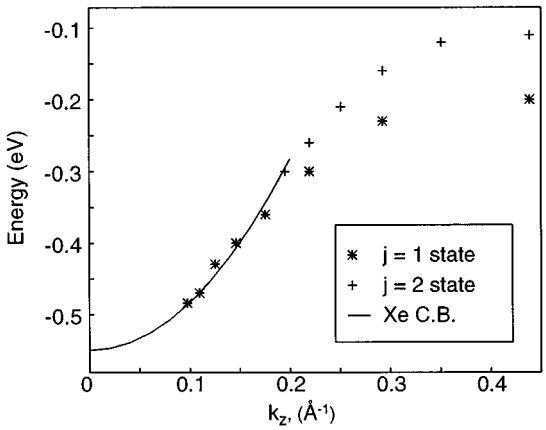

FIG. 7. Perpendicular dispersion plot of Xe quantum well states. The perpendicular wave vector is determined by the layer thickness and the quantum number of the state. The perpendicular dispersion of the $j=1,2$ quantum well states (which correspond to the $n=2,3$ image states) is fit to a parabola, yielding a Xe conduction band minimum of -0.55 eV and an effective mass of 0.57 m_e. The higher k_z values correspond to lower coverage. Energies for the $j=1$ state are plotted versus k_z for 2–9 Xe layers, and energies for the $j=2$ state are plotted versus k_z for 4–9 layers.

ing energies of the $n=2,3$ states are plotted with respect to the perpendicular momentum along with a fit to a parabola determining an experimental value for the Xe conduction band edge of -0.55 eV and an effective mass of $0.57m_e$. Here we have assumed that the $n=2,3$ states are the $j=1,2$ quantum well states, respectively. The binding energies qualitatively match the expected quantum well behavior for 7–9 Xe layers. In the range of 1–3 layers the dispersion is too flat to correspond to a QW state derived from the Xe conduction band, suggesting that $n=2,3$ are modified image states at low coverage. At intermediate coverage the slope of the dispersion curve changes smoothly from flat dispersion to parabolic dispersion, suggesting that the $n=2,3$ states in this range are ''mixed'' states that possess both image state and QW state character, i.e., the wave functions reside in the layer and vacuum to a somewhat equal degree.

It is interesting to note that the crossover between image-like and quantum well-like behavior appears to occur at approximately the thickness corresponding to the expectation value $\langle z\rangle = 6a_0n^2$ for the same state in the hydrogenic image state model[30]—at four layers (14 Å thick) for $n=2$ and at seven layers (25 Å thick) for $n=3$. This result can be interpreted in terms of perturbation theory as follows. For the monolayer, the states are only slightly perturbed from those of the clean surface because of the small spatial overlap of the layer potential with the hydrogenic (zero order) wave function. When the layer is thick enough for significant overlap with the zero order wave function ($t \simeq \langle z\rangle$) , the $n=2,3$ wave functions are brought down in energy by the attractive Xe layer potential. In contrast, the $n=1$ state energy is in the Xe gap, therefore the $n=1$ state is pushed out into the vacuum by the Xe layer.

C. A quantum well on a NFE substrate

We observe that the dielectric model with a hard wall at the metal correctly predicts the gross features of the data but fails quantitatively, especially in that the energies of $n=2,3$ drop too fast as a function of layer thickness. The discrete wave vector model ignores the metal substrate and the image potential in the vacuum. We have developed a simple model which takes into account the important physics of both models and properly treats the electronic structure of the substrate. QW states of a metal layer on a metal substrate have been successfully modeled as a two-band nearly-free-electron (NFE) metal on a two-band NFE substrate with an image potential in the vacuum.[31,32] However, the wide Xe gap with a flat core-level valence band precludes the use of the two-band NFE model for states near the Xe conduction band. It is more proper to ignore the Xe valence band by setting V_{Xe} to the Xe conduction band minimum and using the effective mass approximation for the conduction band dispersion. This recognizes that it is the Xe conduction band which is the origin of the QW states. Therefore we will treat the Ag(111) substrate as an NFE material and construct a potential outside the metal using the effective mass approximation to the Xe conduction band and the image potential outside a dielectric slab on a metal substrate from Sec. IV A.

The particulars of the model are as follows. In the substrate the two-band NFE approximation is used. This approximation has been successful in describing the substrate for the case of surface states in the band gap of a metal. Such states possess an exponential tail in the metal which can be adequately described in the two-band NFE approximation. The notation used here is taken from Ref. 33. In the two-band NFE approximation the crystal potential is written as a Fourier expansion in multiples of the reciprocal lattice vector $\mathbf{g}$, and only the first two terms, $V_{\mathbf{g}}, V_{-\mathbf{g}}$ are kept. For crystals with inversion symmetry $V_{\mathbf{g}} = V_{-\mathbf{g}}$. Electron energies ε with respect to the zero of energy (taken to be the band energy at zone center) for the two-band NFE model are given by solving the secular equation

$$\begin{vmatrix} (\hbar^2/2m^*)\mathbf{k}^2 - \varepsilon & V_{\mathbf{g}} \\ V_{\mathbf{g}} & (\hbar^2/2m^*)(\mathbf{k}-\mathbf{g})^2 - \varepsilon \end{vmatrix} = 0. \tag{10}$$

At the zone boundary at $\mathbf{g}/2$ there is an energy gap of width $2|V_{\mathbf{g}}|$. Within the gap solutions exist for complex k, which correspond to an evanescent wave decaying into the metal. The wave vector can be represented as a sum of real and imaginary components, $k = p + iq$.

For solutions along the surface normal Eq. (10) yields the standard results

$$p = g_z/2, \tag{11}$$

$$(\hbar^2/2m^*)q^2 = (4\varepsilon E_g + V_g^2)^{1/2} - (\varepsilon + E_g), \tag{12}$$

$$E_g = (\hbar^2/2m^*)p^2, \tag{13}$$

$$\sin(2\delta) = -(\hbar^2/2m^*)(pq/V_g), \tag{14}$$

where E_g is the midgap energy, m^* is the effective mass, and $g_z = 2\pi/d$ where d is the interplanar spacing. The wave function in the crystal is given by

$$\psi = e^{qz}\cos(pz + \delta). \tag{15}$$

The sign of $V_{\mathbf{g}}$ depends on the symmetry of the wave function at the top and bottom of the gap. For Ag(111) the band gap is Shockley-inverted: solutions are s-like at the top of the gap and p-like at the bottom. This case corresponds to $V_{\mathbf{g}} > 0$.

We used a value of -0.55 eV with respect to the vacuum for the bulk Xe conduction band minimum and a bulk Xe effective mass of $0.57m_e$ taken from the discrete wave vector analysis in the previous section. The Xe interplanar spacing of 3.577 Å was taken from x-ray data.[21] The Ag(111) parameters were taken from calculations of clean surface image and surface state binding energies.[34] In the vacuum the potential was taken to be the image potential outside a dielectric slab given in Eq. (6) with a cutoff at 1.3 Å from the layer/vacuum boundary. The dielectric constant was fixed at $\epsilon = 2$, which was calculated from the Clausius–Mossotti equation using the atomic polarizability of Xe and the density of solid Xe. An illustration of the potential is given in Fig. 8.

The eigenstates of the model potential were determined by numerical integration as follows. The 2-band NFE solu-

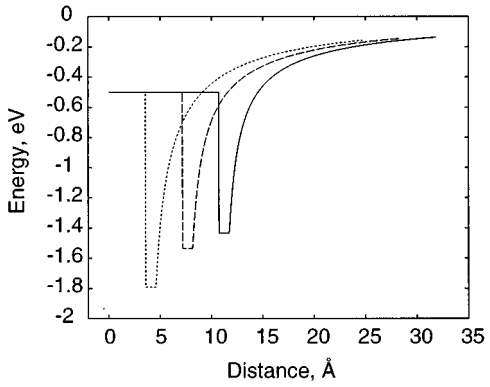

FIG. 8. Potential used in calculating the quantum well states for 1, 2, and 3 layers of Xe. The potential in the layer is set to the Xe conduction band minimum. The potential in the vacuum is the continuum electrostatics solution for an electron outside a dielectric layer on a metal substrate. The model is described in Sec. IV C.

tion for the substrate corresponding to an evanescent wave decaying into the metal substrate is evaluated at the substrate/overlayer interface. The slope and value are then propagated numerically through the flat overlayer potential (where the kinetic energy is evaluated using an effective mass of $0.57m_e$) and out into the vacuum (where the mass is m_e) using a 4th and 5th order Runge–Kutta integrator with adaptive step sizes. The trial solutions are evaluated at large z for a range of energies to find solutions which are ''well-behaved at infinity,'' i.e., eigenstates. The accuracy of this numerical technique was verified by comparison to the results obtained by multiple reflection theory[34] for clean Ag(111) using the potential for the clean surface (i.e., zero layers of Xe).

This model was used to determine binding energies for 1–9 layers of Xe. A cutoff of 1.3 Å in the image potential outside the layer gave the best fit to the data. Binding energies are shown in Fig. 9 and the corresponding probability densities are shown in Fig. 10. The binding energies predicted by the model underestimate slightly the $n=2,3$ binding energies, but the overall agreement with the data is good. The $n=2$ probability density possesses a maximum in the Xe layer, whereas the $n=1$ density exponentially decays within the layer. This is expected since the $n=2$ state is above the Xe gap and thus the wave function propagates (is plane wave-like) in the layer. However, the $n=1$ state is in the Xe gap and does not propagate in the layer.

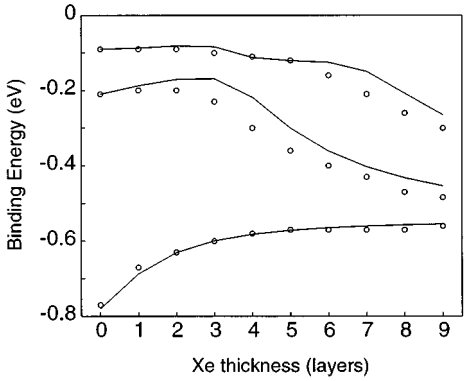

FIG. 9. Comparison between experimental binding energies for the $n=1,2,3$ states for Xe overlayers (symbols) and the predictions of the quantum well model described in Sec. IV C (solid lines).

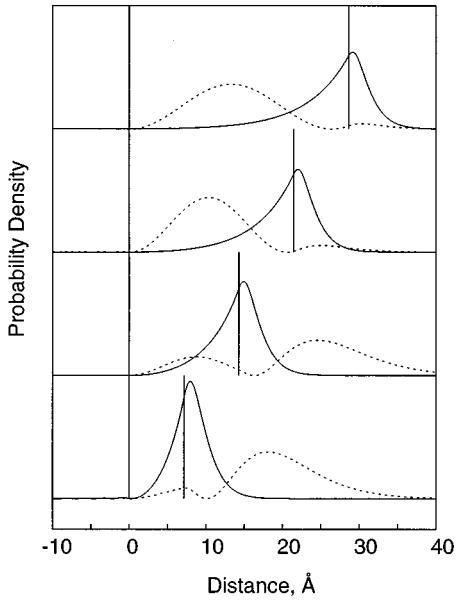

FIG. 10. Calculated probability densities for the $n=1,2$ states for 2,4,6, and 8 layers of Xe/Ag(111) calculated using the model outlined in Sec. IV C for the case of a Xe layer. The vertical lines indicate the thickness of the Xe layer. The solid line represents the $n=1$ state and the dashed line represents the $n=2$ state. The potential used to calculate the wave functions is shown in Fig. 8.

V. DISCUSSION

The coverage dependent spectra exhibited several types of behavior which we attribute to image states, quantum well states, and ''mixed'' states. The $n=1$ state behaves as a screened image state of the composite metal/dielectric interface at intermediate Xe coverage. On the other hand, the $n=2,3$ image states become quantum well states of the overlayer at $7+$ layers of Xe and exhibit a coverage dependence in-between that expected for image and quantum well states for 3–6 layers. An important difference between image states and quantum well states is that image states are energetically within the Xe gap while quantum well states are energetically within the Xe conduction band. Based on this distinction the $n=1$ state, which is below the Xe conduction band in energy, is an image state while the $n=2,3$ states are quantum well states. The image state binding energy depends largely on the electrostatics of the insulator/vacuum interface, while the energy of the quantum well states depends on the perpendicular dispersion and the minimum of the Xe conduction band.

A. Dielectric continuum model

The results of the dielectric continuum model of Sec. IV A indicate that the $n=1$ state moves to more positive binding energy (i.e., weaker binding) due to the dielectric polarization of the Xe slab in the presence of the image potential electron. This is a combination of two competing effects. First, the polarizable Xe adlayer, characterized by dielectric constant ϵ, serves to screen the image electric field between the electron and the metal, leading to a more positive binding energy. Screening is primarily due to the first term in Eq. (2) and the first term in Eq. (6). Second, the induced polarization interaction between the electron and the Xe slab, represented by the second term in Eq. (6), is attractive and favors a more negative binding energy. This model correctly predicts that the net effect for the $n=1$ state is weaker binding to the interface as each of the first five or six layers is added (Fig. 3), which results in a shift of electron density toward the Xe/vacuum interface. This reduction in binding energy is manifest in this model for any case where the affinity of the layer is repulsive with respect to the $n=1$ binding energy. For states above the affinity level in the layer, the state ''falls into'' the layer at some thickness. The fact that the affinity level (Xe conduction band minimum) falls between the $n=1$ and $n=2$ energies separates the coverage dependent behavior of the two states.

B. Relative intensities and lifetime

The relative intensities (Fig. 1) of the peaks as a function of Xe coverage give additional evidence as to the nature of the states. The linewidths would also be important but were difficult to determine due to overlapping features. Photoemission from the $n=1$ state becomes reduced in intensity relative to that from the $n=2,3$ states for 3 and 4 layers of Xe, but is similar in intensity for 6–8 layers of Xe. This is consistent with our assignment of the $n=1$ state to an image state of the Xe layer, primarily located at the vacuum/Xe interface. The intensity of this feature may be determined by two competing effects related to the location of the $n=1$ state at the layer/vacuum interface. The initial decrease in intensity may be due to the fact that the probability of excitation of a substrate electron into the $n=1$ state becomes lower as a function of coverage since the state is located relatively far from the initial states in the metal making the spatial overlap with the bulk states small. Similarly, the increase in relative intensity at 6–8 layers is likely due to an increase in the lifetime of the $n=1$ state. The lifetime increase is due to the fact that the electron must tunnel though a thicker layer in order to decay into the metal.

C. Perpendicular and parallel dispersion

The $n=2,3$ states at higher coverage possess a perpendicular dispersion similar to accepted Xe conduction band values as shown in Fig. 7 and Sec. IV B. The influence of the Xe conduction band can also be seen in the angle-resolved data (Fig. 4), where the dispersion is measured along the surface parallel while the perpendicular momentum is fixed by the layer thickness. The effective masses measured along the surface parallel are higher than accepted bulk Xe conduction band values because for the first few layers a significant fraction of the probability density of the states is in the metal and in the vacuum which has the effect of increasing the effective mass. The effective mass for the $n=1$ image state on a clean Ag(111) surface (corresponding to the limiting case of a state where all the probability density is outside the layer) is $1.3m_e$. The parallel dispersion of the $n=1$ state is free-electron-like for the monolayer ($m^*/m_e=0.95$) and the effective mass monotonically decreases to $m^*/m_e=0.6$ at four layers. Also apparent from Fig. 4 is that, for a given layer thickness, the $n=1$ state has a lower effective mass (closer to the bulk Xe value of $0.35m_e$)[35] than that of the $n=2$ state. This may be due to differences in the spatial overlap of the states with the substrate and overlayer. According to our calculations in Sec. IV C the $n=2$ state has a higher probability density in the metal than $n=1$ which should increase the effective mass with respect to $n=1$. The probability densities for two and four layers (Fig. 10) show that, for up to four layers, the $n=1$ state has more electron density in the layer than does the $n=2$ state.

It should be noted that the high energy and momentum resolution afforded by this technique along both the surface parallel and surface normal yield the most precise, detailed spectra to date of the Xe conduction band. Angle-resolved UPS of a bulk single crystal conducted at a variety of wavelengths can also map out the conduction band structure, but UPS resolution is ultimately limited by hole lifetime effects and the fact that k_z is only partially conserved in photoemission from bulk material.

D. QW on a NFE substrate

Our QW treatment is guaranteed to reproduce the clean surface results in the limit of zero coverage and the perpendicular dispersion of the Xe conduction band in the limit of a very thick Xe layer. It also appears to adequately describe the data of some (the $n=2,3$) states in the intermediate case of 1–9 layers. The probability density of the wave functions in Fig. 10 indicates that for two Xe layers approximately 5% of the $n=2$ wave function is in the layer whereas for 8 atomic layers of Xe approximately 95% of the wave function is in the layer. The QW treatment is perhaps successful because it partitions the wave function more or less correctly between the layer, vacuum, and substrate, allowing the substrate and vacuum parts of the potential to primarily determine the $n=2,3$ binding energy for the first few layers but allowing the overlayer potential to dominate for thicker layers.

Merry *et al.*[14] discussed the effect of the work function shift due to adsorption on the image state binding energy. In our application of this model, we took into account the work function shift of -0.5 eV. Therefore this effect of the substrate band structure is explicitly accounted for in this model, allowing for a comparison of the relative importance of the work function shift, the dielectric layer, and the band structure of the layer.

VI. CLOSING COMMENTS

The binding energies and effective masses of the excited states of the Xe/Ag(111) interface within an electron-volt below the vacuum level have been measured using ARTPPE for one to nine atomic layers. Purely 2-D image potential states (which only propagate freely in the plane of the surface) evolve into quantum well states that converge to the conduction band states of the 3-D bulk xenon solid with increasing layer thickness. This work demonstrates that ARTPPE is a powerful technique for studying the transition from two- to three-dimensional electronic structure at nanometer scale interfaces. We conclude that the simple QW model outlined in Sec. IV C accounts for the energies of the $n=1,2,3$ states over the range of coverages examined in this work. Work has been done to extend the time resolution of this technique to <100 fs.[13] These ultrafast measurements of electron dynamics as a function of parallel and perpendicular momentum should lead to a better understanding of charge transport across interfaces involving dissimilar materials and low-dimensional electronic structures.

ACKNOWLEDGMENTS

We are grateful to N.-H. Ge for experimental assistance and to Neville Smith for helpful discussions on modeling quantum wells. This work was supported by the Director, Office of Energy Research, Office of Basic Energy Sciences, Chemical Sciences Division of the U. S. Department of Energy, under Contract No. DE-AC03-76SF00098.

[1] M. L. Klein and J. A. Venables, *Rare Gas Solids* (Academic, London, 1976–1977).
[2] W. A. Harrison, *Electronic Structure and the Properties of Solids* (Dover, New York, 1989).
[3] P. D. Loly and J. B. Pendry, J. Phys. C **16**, 423 (1983).
[4] M. A. Mueller, T. Miller, and T.-C. Chiang, Phys. Rev. B **41**, 5214 (1990).
[5] A. L. Wachs, A. P. Shapiro, T. C. Hsieh, and T.-C. Chiang, Phys. Rev. B **33**, 1460 (1986).
[6] M. Jalochowski, H. Knoppe, G. Lillenkamp, and E. Bauer, Phys. Rev. B **46**, 4693 (1992).
[7] T. Schmitzhubsch, K. Oster, J. Radnik, and K. Wandelt, Phys. Rev. Lett. **74**, 2595 (1995).
[8] K. Giesen, F. Hage, H.J. Reiss, W. Steinmann, R. Haight, R. Beigang, R. Dreyfuss, Ph. Avouris, and F.J. Himpsel, Phys. Scr. **35**, 578 (1987).
[9] K. Giesen, F. Hage, F. J. Himpsel, H. J. Reiss, W. Steinmann, and N. V. Smith, Phys. Rev. B **35**, 975 (1987).
[10] R. Haight, Surf. Sci. Rep. **21**, 275 (1995).
[11] R. W. Schoenlein, J. G. Fujimoto, G. L. Eesley, and T. W. Capehart, Phys. Rev. Lett. **61**, 2596 (1988).
[12] R. W. Schoenlein, J. G. Fujimoto, G. L. Eesley, and T. W. Capehart, Phys. Rev. B **41**, 5436 (1990).
[13] R. L. Lingle, N.-H. Ge, R. E. Jordan, J. D. McNeill, and C. B. Harris, Chem. Phys. **205**, 191 (1996).
[14] W. R. Merry, R. E. Jordan, D. F. Padowitz, and C. B. Harris, Surf. Sci. **295**, 393 (1993).
[15] D. F. Padowitz, W. R. Merry, R. E. Jordan, and C. B. Harris, Phys. Rev. Lett. **69**, 3583 (1992).
[16] R. L. Lingle, D. F. Padowitz, R. E. Jordan, J. D. McNeill, and C. B. Harris, Phys. Rev. Lett. **72**, 2243 (1994).
[17] R. Fischer, Th. Fauster, and W. Steinmann, Phys. Rev. B **48**, 15496 (1993).
[18] R. Fischer and Th. Fauster, Phys. Rev. B **51**, 7112 (1995).
[19] J. Unguris, L. W. Bruch, E. R. Moog, and M. B. Webb, Sur. Sci. **87**, 415 (1979).
[20] J. Unguris, L. W. Bruch, E. R. Moog, and M. B. Webb, Sur. Sci. **109**, 522 (1981).
[21] P. Dai, T. Angot, S. N. Ehrlich, S. K. Wang, and H. Taub, Phys. Rev. Lett. **72**, 685 (1994).
[22] R. H. Fowler, Phys. Rev. **38**, 45 (1931).
[23] R. J. Behm, C. R. Brundle, and K. Wandelt, J. Chem. Phys. **85**, 1061 (1986).
[24] M. W. Cole, Phys. Rev. Lett. **23**, 1238 (1969).
[25] M. W. Cole, Phys. Rev. B **3**, 4418 (1971).
[26] B. Trninić-Radja, M. Šunjić, and Z. Lenac, Phys. Rev. B **40**, 9600 (1989).
[27] T. R. Brown and J. C. Grimes, Phys. Rev. Lett. **9**, 1233 (1972).
[28] J. D. Jackson (private communication).
[29] M. Michaud, P. Clautier, and L. Sanche, Phys. Rev. B **44**, 10485 (1991).
[30] P. M. Echenique and J.B. Pendry, J. Phys. C **11**, 2065 (1978).
[31] N. V. Smith, N. B. Brookes, Y. Chang, and P. D. Johnson, Phys. Rev. B **49**, 332 (1994).
[32] J. E. Ortega, F. J. Himpsel, G. J. Mankey, and R. F. Willis, Phys. Rev. B **47**, 1540 (1993).
[33] N. V. Smith, Phys. Rev. B **32**, 3549 (1985).
[34] P. M. Echenique and J. B. Pendry, Prog. Surf. Sci. **32**, 111 (1990).
[35] U. M. Grassano and N. Terzi, *Excited-State Spectroscopy in Solids* (North-Holland, New York, 1987).